



HAL
open science

Reversible microfluidics device for precious metal electrodeposition and depletion yield studies

Jérémie Gouyon, Craig Simon, Sophie Griveau, Catherine Sella, Laurent Thouin, Fethi Bedioui, Anne Varenne

► **To cite this version:**

Jérémie Gouyon, Craig Simon, Sophie Griveau, Catherine Sella, Laurent Thouin, et al.. Reversible microfluidics device for precious metal electrodeposition and depletion yield studies. *Electrochimica Acta*, 2020, 10.1016/j.elecom.2017.05.013 . hal-03021320

HAL Id: hal-03021320

<https://hal.science/hal-03021320>

Submitted on 24 Nov 2020

HAL is a multi-disciplinary open access archive for the deposit and dissemination of scientific research documents, whether they are published or not. The documents may come from teaching and research institutions in France or abroad, or from public or private research centers.

L'archive ouverte pluridisciplinaire **HAL**, est destinée au dépôt et à la diffusion de documents scientifiques de niveau recherche, publiés ou non, émanant des établissements d'enseignement et de recherche français ou étrangers, des laboratoires publics ou privés.

1 **Flow-based microchip for precious metal electrodeposition and depletion yield studies**

2 Jérémie Gouyon ^{1,2}, Fanny d'Orlyé ¹, Craig Simon ^{1,3}, Sophie Griveau ¹, Catherine Sella ⁴,
3 Laurent Thouin ⁴, Fethi Bedioui ¹, Anne Varenne ^{1*}

4 ¹ Chimie ParisTech, PSL University, CNRS 2027, Institute of Chemistry for Life and Health Sciences, SEISAD 75005 Paris,
5 France.

6 ² French Environment and Energy Management Agency, 20, avenue du Grésillé- BP 90406 49004 Angers Cedex 01, France

7 ³ University of Strathclyde, Glasgow G1 1XQ, United Kingdom

8 ⁴ PASTEUR, Département de chimie, École normale supérieure, PSL Université, Sorbonne Université, CNRS, 75005 Paris,
9 France

10 E-mail: anne.varenne@chimieparistech.psl.eu (Varenne A.)

11 **Abstract**

12 A new low-cost reversible Glass-NOA[®]-PDMS microfluidic device was designed for the study of
13 recovery yield of precious metals present in acid media mimicking leach liquors for long-term
14 recycling objectives. It offers the unique advantage of allowing easy washing of the microchannel
15 and renewal of the electrode surface by simply repositioning the microband electrodes. It consists
16 in a re-usable microchip with four graphite microbands electrodes, prepared by screen printing, to
17 set-up an original amperometric device for both depletion and yield quantification. One upstream
18 working electrode is devoted to the depletion of the metallic ions through their electrolysis by
19 electrodeposition while the second downstream working microelectrode is used as real-time
20 detection electrode to evaluate the depletion efficiency. The dimensions of the depletion electrode
21 and of the channel were optimized thanks to numerical simulations for a given range of flow
22 velocities. First, the performances of the device were assessed experimentally according to flow

23 rate and applied potential under continuous flow, and then compared to theoretical predictions
24 using an electrochemical probe, ferrocenemethanol. The proof of concept was then demonstrated
25 for precious metal, by electroreduction of Pd(II) and Au(III) from acidic leach liquors under
26 continuous flow, with a depletion yield of up to 89% and 71% respectively.

27 **Keywords**

28 Precious metals – Microfluidic – Depletion – Electrodeposition – Recycling

29 **1. Introduction**

30 Printed circuit boards (PCBs) are known as an integral part of our technological devices
31 (smartphones, computers...). As their use has become more and more important in the recent
32 decades, the amount of waste is increasing and becomes an ecological, economic and strategic
33 challenge [1,2]. Indeed, waste PCBs are a major source of strategic metals [3], such as platinum
34 group metals (PGM), rare earth elements or other expensive species. Their recovery is crucial,
35 especially since some of them are defined as critical (supply risks, high cost) by the European
36 Commission [4] since 2014, such as Platinum (Pt) or Palladium (Pd). Their recycling is generally
37 carried out in a three steps process [5]: (i) a mechanical grinding to reduce PCBs to powders and
38 separate ferrous and non-ferrous metals, (ii) pyrolysis at 1000°C to remove the organic
39 constituents and (iii) a hydrometallurgical treatment to selectively remove metals in ionic form in
40 leaching solutions. These treatments are thus promising in terms of strategic metals recovery rate,
41 but purification methods are still time-consuming and need to be optimized to ensure high purity
42 of recycled materials, especially in their metallic form.

43 Thanks to microfluidics [6], the change in scale from an industrial process to microchannel
44 results in a modification of the mechanical properties of fluids. This allows leading to high

45 conversion for organic synthesis, for example, and high purity of the products [7,8]. In addition,
46 the low manufacturing cost of microreactors permits them to be parallelized, allowing for
47 processing a large quantity of samples, thus competing with current industrial macro-processes
48 [9]. Even if diagnosis is one of the main application of microfluidics (for environmental [10] and
49 biological [11] survey), the use of such miniaturized tools for the treatment of large amounts of
50 liquid is also feasible.

51 Microfluidic coupled to the integration of electrodes within microchannels has been previously
52 used to remove potential interfering agents from real samples but also to increase the selectivity
53 towards a target (such as oxalic acid or nitric oxide) during its electrochemical detection [12,13].
54 The developed setups are composed of a four-electrodes cell, where two working electrodes
55 (WE) are placed perpendicularly to a single microchannel containing the solution under
56 continuous flow. Watanabe et al. [12] used a large WE (WE_{DEP} , depletion electrode) in order to
57 remove the electroactive analyte (ferricyanide) from the solution and checked the depletion yield
58 by measuring ferricyanide concentration thanks to the second WE (WE_{det} , detection electrode)
59 positioned downstream. The importance of main parameters on the depletion yield has been
60 discussed by the authors such as ratio of electrode width to channel height, flow velocity and
61 applied potentials. The authors stated that their setup was not suitable to complete the depletion
62 up to 100 % due to the height of the channel which was larger than the convection-diffusion layer
63 of the sample. Indeed, the thin-layer regime at the electrode must be achieved under mass
64 transport control for complete depletion [14–16]. More recently, similar strategy was adopted for
65 the assessment of global antioxidant capacity and for the depletion of hydrogen peroxide (up to
66 95%) [13]. In this last case, the selectivity of nitric oxide detection was enhanced by positioning a
67 NO-sensor downstream of the depletion electrode. **It should be noted that the devices described in**

68 the literature for this type of application are sealed and do not offer any possibility of easy and
69 quick reuse in case of pollution of the depletion electrodes and their regeneration.

70 Reversibly bonded chips were reported in the literature and they were generally used for other
71 applications such as coupling of electrophoresis with electrochemical detection or surface
72 patterning for bio-molecule analysis [17]. Several strategies for the reversible bonding of the
73 different parts of the microdevices were used such as magnetism, vacuum or spontaneous
74 conformal contact between PDMS and glass [18] or other materials (metals, acrylic plate [19]).
75 They offer the main advantage of facilitating the washing and the renewability of channels. We
76 propose in this study an original microfluidic device to address the issue of recovering Au and Pd
77 dissolved in acidic media (as AuCl_4^- and PdCl_4^{2-} respectively), mimicking leach liquors from the
78 waste PCBs recycling process. For this purpose, a re-usable new reversible Glass-NOA[®]-PDMS
79 microchip with four graphite microbands electrodes adapted from previously developed one by
80 our group [20], was designed to set-up an original amperometric recovery device for both
81 depletion and yield quantification. The device reported here offers the unique advantage of being
82 a micro sandwich system with a reversible bond composed of two parts without the need for a
83 magnetic or other device to maintain perfect adhesion, allowing easy washing of the
84 microchannel and renewal of the electrode surface by simply repositioning the microband
85 electrodes. This configuration permits enhancing its lifetime. First, to optimize the performance
86 of the proposed microdevice, ferrocene methanol was used as a model. Then, the method
87 efficiency for precious metallic species were discussed and compared to theoretical predictions.

88 **2. Materials and methods**

89 *2.1. Chemicals*

90 Standard solution of Gold Standard for ICP TraceCERT® 1000 mg/L (5% HCl) and Palladium
91 Standard for ICP TraceCERT® 10000 mg/L (10% HCl with HNO₃⁻ traces), ferrocene methanol
92 (noted as FcMeOH, 97%), sodium phosphate dibasic (99%), sodium phosphate monobasic (99%)
93 were purchased from Sigma-Aldrich (Germany). HCl (37%) was purchased from Acros Organics
94 (France). Graphite powder (2-15µm microcrystal grade 99.9995%) was obtained from Alfa Aesar
95 (Germany), PDMS RTV 615 kit was obtained from Mentiv (France), PDMS Sylgard 184 kit
96 from Dow Corning (Germany), SU8 2075 from Microchem (USA), and Norland Optical
97 Adhesive 81[®] (noted as NOA81[®]) from Epotecnny (France) and were used for fabrication of
98 microchannels and microelectrodes. Ultrapure water was obtained from a Purelab Flex System
99 (18.2 MΩ.cm Veolia, France).

100 *2.2. Solutions*

101 The artificial leach liquors were prepared by dilution of appropriate amounts of metallic standard
102 solutions with HCl in ultrapure water so as to obtain a 0.1 mol L⁻¹ HCl solution. 200 µmol L⁻¹
103 FcMeOH was prepared in 0.2 mol L⁻¹ phosphate buffer (pH 6.7) with sonication for at least 2
104 hours to complete solubilization.

105 *2.3. Microelectrode and microchip fabrication*

106 The microfabrication process, developed in our lab, has been previously described [20]. Briefly,
107 for the electrode fabrication, PDMS substrates containing microchannels of desired width are
108 prepared by soft-lithography technic. A pattern is molded by UV exposure of spin-coated SU-8
109 on a silicon wafer with a photomask containing the design of the electrodes. Electrode pattern

110 were printed on Kimolek® Paper with a Filmstar® photoplotter (Bernier Electronik, France).
111 PDMS is spread on the surface of the mold prior to degassing and reticulating at 70°C for 1h. A
112 mix of graphite powder and PDMS (C-PDMS, 1:1, w/w) is spread in the microchannels and
113 polished by hand to remove the excess. The resulting electrodes are placed in an oven at 70°C for
114 3h before use. For the microchannel fabrication, a PDMS mold containing the positive pattern is
115 prepared by the same technic. The mold is applied on top of a glass substrate previously covered
116 with NOA®81. After UV exposure, the open-channel is revealed by properly demolding the
117 PDMS mold. The two part are then assembled so as to close the chip, forming a spontaneous
118 conformal contact between the open-channel (NOA81®) and the electrode (C-PDMS on PDMS
119 substrate). The scheme and a picture of the setup are shown in Figure 1. In such a device, WE_{DEP}
120 is the working electrode dedicated to the depletion process (and also to the recovery of the
121 metals), WE_{det} is the working electrode dedicated to the determination of the considered species
122 and thus to the evaluation of the recovery efficiency.

123
124 **Figure 1 – (a) Scheme of microchannel with four integrated C/PDMS microbands**
125 **electrodes. WE_{DEP} is dedicated to the depletion process (and thus to the recovery), WE_{det} is**
126 **dedicated to the determination of the considered species and thus to the evaluation of the**
127 **recovery efficiency. Dimensions in μm (unless specified). * upper part of the setup (NOA81®**
128 **microchannel; ** lower part of the setup (C-PDMS electrodes in PDMS substrate) (b)**
129 **Photography of the experimental setup**

130 2.4. Electrochemical measurement and depletion

131 Chronoamperometric (CA) and cyclic voltammetric (CV) measurements were performed with an
132 Autolab PGSTAT 128N potentiostat (Metrohm), in a four electrodes cell (two WE coupled to one
133 reference electrode RE and one counter electrode CE). The CVs were performed at 25 mV s⁻¹ for
134 each electrode to determine the potential required for CA, with RE connected to the 100 μm strip

135 electrode and the CE connected to the 1000 μm strip electrode. The WE dedicated to the
136 depletion (WE_{DEP}) was located upstream (500 μm width) along the flow direction, and the one
137 dedicated to detection for control (WE_{det}) was positioned downstream (50 μm width). The flow of
138 the solution along the microchannel was insured by a flow controller (MFCSTM-EZ and flow rate
139 sensor S, Fluigent, France), applying a negative pressure (0 to -345 mbar) from the outlet of the
140 channel to prevent detachment of the reversibly sealed chip. The depletion yield for FcMeOH, Pd
141 and Au were estimated by measuring in CA the difference in oxidation charge generated on the
142 WE_{det} with and without polarization of WE_{DEP} , after subtraction of charges measured with a
143 blank sample (phosphate buffer or HCl alone). The depletion yield for FcMeOH was also
144 evaluated from steady-state currents in CV.

145 The dimensions of the channels and of the electrode as well as the estimation of the depletion
146 yield were first optimized by performing numerical simulations using COMSOL Multiphysics
147 5.3, through a similar approach as previously described [13]. Briefly, a laminar flow was
148 considered in a rectangular microchannel by assuming a parabolic velocity profile in a two-
149 dimension. The electrochemical reactions were supposed to be limited by mass transport and the
150 diffusion-convection equation was solved numerically by finite elements. As a boundary
151 condition, concentration of the analyte was imposed to 0 mol L⁻¹ at the polarized electrode
152 surface. The diffusion coefficient of the analyte was assumed equal to $7.6 \cdot 10^{-6}$ cm² s⁻¹, which is
153 the one of FcMeOH used as a model [21]. Simulations provided an optimal size of WE_{DEP} versus
154 the channel height, within the range of flow velocities that could be used experimentally.
155 According to the configuration and geometry of the microdevice described in Figure 1, depletion
156 yields up to 95 % were expected for flow rate lower than 2 $\mu\text{L min}^{-1}$. The device was then applied
157 to the recovery of Pd(II) and Au(III).

158 3. Results and discussion

159 3.1. Electrochemical behavior of FcMeOH under continuous flow

160 The electrochemical behavior of FcMeOH has been studied in the present configuration by CV
161 on both WEs without flow (static mode) and under continuous flow (from 1 to 5 $\mu\text{L min}^{-1}$), as
162 shown on Figure 2. The oxidation current for both WEs (WE_{DEP} and WE_{det}) increase with the
163 flow rate due to convection induced by continuous flow, leading to a steady-state mass transport
164 to the electrodes and the observation of limiting currents. As expected in convective regimes,
165 limiting currents increase linearly with the cubic root of flow rate (see inserts). At the highest
166 flow rate (5 $\mu\text{L min}^{-1}$, *i.e.* 2.1 mm s^{-1}), the faradic current started from about 0.1V and reached a
167 limiting value only for potential values higher than 0.5V due mainly to ohmic drop. According to
168 these voltammograms the potential on both electrodes should be comprised between +0.5 and
169 +1.0 V to ensure a constant oxidation current under continuous flow (for 1 to 5 $\mu\text{L min}^{-1}$) for
170 optimal operating conditions. Indeed, to guarantee an optimum depletion efficiency (see sections
171 below), the process needs to be performed at potential values that do not lead to a drastic current
172 variation.

173 **Figure 2 – Cyclic voltammograms of 200 $\mu\text{mol L}^{-1}$ FcMeOH in 0.2 mol L^{-1} phosphate buffer**
174 **at (a) WE_{DEP} and (b) WE_{det} , in static mode (full line) and under continuous flow (from 1 to**
175 **5 $\mu\text{L min}^{-1}$). Scan rate: 25 mV s^{-1} . Inserts correspond to the plots of limiting currents as a**
176 **function of cubic root of flow rate.**

177 3.2. FcMeOH depletion

178 Cyclic voltammograms (CV) were performed at WE_{det} with and without polarization of WE_{DEP} at
179 a constant potential of +1.0 V. Figure 3-a shows the mean values of limiting currents, noted as
180 $I_{\text{lim,WEdet}}$, monitored under these conditions at WE_{det} as a function of flow rate. The depletion

181 yield (Figure 3-b) was determined from these data by calculating the ratio between limiting
182 currents at WE_{det} (corrected from residual currents) with and without polarization of WE_{DEP}:

$$Depletion\ yield_{CV}\ (\%) = \left(1 - \frac{I_{lim, WE_{det}}\ with\ WE_{DEP}^{ON}}{I_{lim, WE_{det}}\ with\ WE_{DEP}^{OFF}} \right) \times 100 \quad eq.1$$

183 As expected theoretically, the depletion yield decreases by increasing the flow rate: the higher the
184 flow, the shorter the residence time of redox species near the depletion electrode. However,
185 experimental depletion yields were lower (by a factor ranging between 1.2 to 2) than the ones
186 predicted by simulation, as shown in Figure 3-b.

187 **Figure 3 – (a) Limiting currents measured by cyclic voltammetry (from data in Fig. 2) at**
188 **WE_{det} without (OFF) and with (ON) polarization of WE_{DEP}. (b) Corresponding depletion**
189 **yield evaluated from eq.1 as a function of flow rate. WE_{DEP} is biased at 1.0 V when**
190 **polarized (ON).**

191 The depletion process was also evaluated by chronoamperometry (CA). More precisely,
192 consecutive potential steps (ON) and (OFF) were performed at WE_{DEP}, while maintaining WE_{det}
193 at a constant potential of 1 V for oxidizing remaining FcMeOH (Figure 4). Note that polarization
194 of WE_{DEP}, at 1 V and 0 V corresponds to the activation (ON) and deactivation (OFF) of the
195 depletion process, respectively. As expected, polarization of WE_{DEP} at +1,0V leads (i) to the
196 increase of currents characteristic of FcMeOH oxidation and (ii) to a decrease of currents at
197 WE_{det} due to FcMeOH depletion. With this configuration of device and electrode material, the
198 time delay to reach steady-state currents was estimated about 10 s.

199 **Figure 4 – (a) Potential steps applied to WE_{DEP} for successive activations (1 V) and**
200 **deactivations (0 V) of the depletion process. WE_{det} is continuously polarized at 1 V. (b)**
201 **Corresponding chronoamperograms monitored at WE_{det} (full line) and WE_{DEP} (dashed**
202 **line). 200 μmol L⁻¹ FcMeOH in 0.2 mol L⁻¹ phosphate buffer and flow rate of 1 μL min⁻¹.**

203 Then, similar experiments were conducted on a longer time scale. Figure 5-a shows
204 chronoamperograms obtained at WE_{det} for low flow rate (1 μL min⁻¹, i.e. 0.4 mm s⁻¹) with or

205 without polarization of WE_{DEP}. First, a potential of 0 V was applied to WE_{det} during 30 s for
 206 stabilization of the baseline followed by a potential step to 1.0 V during 60 s. This procedure was
 207 applied either in presence of FcMeOH or in PBS to consider the influence of residual currents
 208 into the evaluation of the charges developed at WE_{det}, noted as Q_{WE_{det}}. Experiments were also
 209 carried out for other flow rates. Thus Figure 5-b shows the evolution of Q_{WE_{det}} during the second
 210 step as a function of flow rate, with or without polarization of WE_{DEP}. These data allowed
 211 evaluating in Figure 5-c the corresponding depletion yields (with subtraction of charge measured
 212 in PBS) according to the equation

$$Depletion\ yield_{CA}\ (\%) = \left(1 - \frac{Q_{WE_{det}}\ with\ WE_{DEP}^{ON}}{Q_{WE_{det}}\ with\ WE_{DEP}^{OFF}} \right) \times 100 \quad eq.2$$

213

Figure 5 – (a) Chronoamperometry at WE_{det} (30 s at 0 V and 60 s at 1.0 V) without depletion (curves 1 and 2, WE_{DEP} OFF) and with depletion (curves 3 and 4, WE_{DEP} polarized at 1 V) at 1 μL min⁻¹ flow rate. (b) Experimental charge Q_{WE_{det}} developed at WE_{det} during the second step as a function of flow rate. (c) Depletion yield evaluated by eq. 2 from experimental data (cross points, dashed line) and simulations (solid curve) as a function of flow rate (200 μmol L⁻¹ FcMeOH in 0.2 mol L⁻¹ phosphate buffer).

214 In comparison to data obtained by CV (Figure 3-b) the same behavior was observed as a function
 215 of flow rate. A maximal depletion yield of 76.4% at the lowest flow rate 1 μL min⁻¹. The
 216 discrepancy between experimental and simulated data was similar. Indeed, the experimental
 217 depletion yields were lower than the predicted ones with: 76.4±3.3 % versus 99.6 at 1 μL min⁻¹
 218 and 41.1±7.0 % versus 73.4 % at 4 μL min⁻¹. As for data obtained by CV, this can be attributed to
 219 the composite material C-PDMS of the electrodes that does not lead to a well-defined active
 220 surface, perfectly planar, homogeneous, with no cavity or deformation. As shown by SEM [20],
 221 the C-PDMS electrodes cannot be considered as planar for simulations. Also, the ohmic drop can
 222 reduce the performances of the depletion process if steady-state current at WE_{DEP}, related to

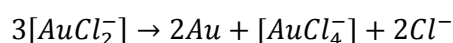
223 mass-transport limitation, is not reached at the applied potential. The larger the WE_{DEP} ; the higher
224 the influence of ohmic drop on depletion yield. However, according to our previous experiments,
225 the potential of 1.0 V that was applied at both electrodes was sufficiently high to overcome the
226 ohmic drop and to implement a process fully limited by mass transport. Therefore, only surface
227 defaults and inactive areas of the C-PDMS electrodes could explain the deviations observed from
228 numerical simulations.

229 Compared to the previously mentioned literature [13], performance of this microdevice is lower.
230 In our case, the electrode material and aspect lead to significant differences since simulation did
231 not consider the exact shape and nature of the material, and thus cannot reach the same level of
232 efficiency than other metal electrode material. But since **this system is low fabrication cost**, C-
233 PDMS electrode material is of interest to counteract the onerous and technically laborious
234 development of platinum electrodes. Also the eventual electrode passivation after successive runs
235 and its potential pollution are overcompensated by the originality of **this reversible** system.
236 **Indeed, in case of major pollution of the electrodes during depletion processes, the device can be**
237 **re-used as many times as portions of the band electrodes have not been exposed to the electrolyte**
238 **solution. This is clearly an advantage compared to previously developed irreversibly closed**
239 **depletion systems.**In the case of FcMeOH study, no passivation was observed for the duration of
240 the study on the different electrode areas used **as continuous monitoring of blank samples was**
241 **performed between each analysis so as to check the electrode and eventually renew the**
242 **electroactive surface to avoid potential deterioration of the system.**

243 *3.4. Electrochemical reduction of chlorocomplexes of gold and palladium*

244 The electrochemical activity of the different metal complexes has been previously examined on
245 glassy carbon electrode in HCl solution [22,23], with electrodeposition occurring for potential

246 value of 0 V for Pd and 0.35 V for Au. Pd and Au in HCl solution can be reduced and metals can
247 be deposited according to the following reactions:



248 Their electrodeposition on C-PDMS microelectrode within a microchannel occurs similarly but at
249 different potentials (about -0.3 V and -0.5 V/C-PDMS for Au and Pd, respectively, Figure 6). The
250 difference in values is due to the use of the pseudo-reference C-PDMS and to the nature of the C-
251 PDMS electrodes. The stripping processes take place at around 0.26 and 0.30 V/C-PDMS for Au
252 and Pd respectively, with behaviors similar to those described on glassy carbon electrodes. At 1
253 $\mu\text{L min}^{-1}$, the voltammograms on both WE_{DEP} and WE_{det} for Au and Pd do not show a wave-
254 shaped signal, except for Au on WE_{det} (Figure 6-a). Indeed, the presence of a metal deposit on C-
255 PDMS electrode such as Pd catalyzes hydroxonium ions reduction, leading to the overlapping of
256 reduction signals and possibly to some interferences, as it will be discussed later.

257
258 **Figure 6 – Cyclic voltammograms of (a) 500 $\mu\text{mol L}^{-1}$ Au in 0.14 mol L^{-1} HCl and (b) 1000**
259 **$\mu\text{mol L}^{-1}$ Pd in 0.1 mol L^{-1} HCl on WE_{det} and WE_{DEP} at 25 mV s^{-1} (static mode)**

260 3.5. Au and Pd electrodeposition as a function of applied potential and flow rate

261 Experiments were performed by chronoamperometry within the microchannel under constant
262 flow rate (1 $\mu\text{L min}^{-1}$) for different potentials. The deposition yields of both metals were
263 evaluated separately. Three potential steps were successively applied at WE_{DEP} and at WE_{det} : (i) 0
264 V for 30 s to evaluate the current baseline, (ii) a constant potential between -0.4 and -1.2 V for 60

265 s to reduce metal ions and finally (iii) +0.5 V for more than 100 s to fully oxidize the metal
266 deposits.

267 Figure 7 shows the chronoamperograms obtained at WE_{det} with the corresponding oxidation
268 charges (third step) at both WE_{DEP} and WE_{det} as a function of the applied potential for metal
269 reduction.

Figure 7 – (a) Chronoamperograms (i & ii) of $1000 \mu\text{mol L}^{-1}$ Pd in 0.1 mol L^{-1} HCl and $500 \mu\text{mol L}^{-1}$ Au in 0.14 mol L^{-1} HCl at WE_{det} under $1 \mu\text{L min}^{-1}$ flow rate with WE_{DEP} polarized at various potential and (b) oxidation charges corresponding to the third step measured at WE_{det} and on WE_{DEP} as a function of the reduction potential applied to WE_{DEP} during the second step.

270
271 The depletion yield as a function of flow rate for both metals is given in Figure 8. The same
272 experiment than figure 7 was performed but without activation of WE_{DEP} so as to estimate the
273 depletion yield, calculated from the oxidation charges Q developed at WE_{DEP} and WE_{det} during
274 the third step as follows:

$$Depletion\ yield_{CA}\ (%) = \left(1 - \frac{Q_{WE_{det}}\ with\ WE_{DEP}^{ON}}{Q_{WE_{det}}\ with\ WE_{DEP}^{ON}} \right) \times 100 \quad eq.5$$

275 Note that the calculation of the depletion yield was not based on cathodic charges because the
276 metal reductions are prone to interferences from solvent reduction. The highest depletion yields
277 were obtained for the lowest flow rates, as previously observed for FcMeOH, namely 68.2 and
278 44.6 % for Au and Pd, respectively at $1 \mu\text{L min}^{-1}$.

279 **Figure 8 – Depletion yield estimated from Eq. 5 for Pd and Au as a function of the flow rate.**
280 **($500 \mu\text{mol L}^{-1}$ Au in 0.14 mol L^{-1} HCl, 1 mmol L^{-1} Pd in 0.1 mol L^{-1} HCl, $200 \mu\text{mol L}^{-1}$**
281 **FcMeOH in phosphate buffer 0.2 mol L^{-1} , first step (0 to 30 s): $WE_{det} = 0 \text{ V/C-PDMS}$;**
282 **second step (30 to 90 s): $WE_{det} = -1 \text{ V}$, -1.2 V and $+1 \text{ V/C-PDMS}$ for Au, Pd and FcMeOH,**
283 **respectively, and third step (90 to 200 s): $WE_{det} = 0.5 \text{ V/C-PDMS}$ (for Pd and Au, only).**
284 **WE_{DEP} is set at the same potential than WE_{det} when activated.**

285 *3.6. Depletion yield as a function of metal concentration and mechanism of deposition*

286 The previously described results allowed setting the optimum parameters for the depletion of
287 precious metals as follows: reduction potential values of -1.0 and -1.2 V for Au and Pd,
288 respectively and minimal flow rate of 1 $\mu\text{L min}^{-1}$. The evaluation of the depletion yield as a
289 function of the metal concentration in acidic solution was then performed (Figure 9) using the
290 same procedure as in Figure 8 for concentrations ranging between 25 and 500 $\mu\text{mol L}^{-1}$ for Au
291 and for concentrations ranging between 25 to 1000 $\mu\text{mol L}^{-1}$ for Pd.

292 **Figure 9 – Depletion yield of Au and Pd as function of their concentration for flow rate of 1**
293 **$\mu\text{L min}^{-1}$. Same conditions as in Figure 8.**

294 The data showed that the depletion yield decreased with the increase in concentration for both
295 metals, with values of up to 89% for Pd (25 $\mu\text{mol L}^{-1}$ / 2.7 mg L^{-1}) and 71 % for Au (25 $\mu\text{mol L}^{-1}$
296 / 4.9 mg L^{-1}). These results are promising since they are obtained for concentrations close to the
297 expected ones in real leach liquors from waste printed circuits boards recycling processes (9.4 to
298 94.0 mg L^{-1} for Pd and 5.1 to 50.8 mg L^{-1} for Au) [24].

299 Simulations performed under similar conditions predicted a depletion yield of 89% at 2.6 $\mu\text{L min}^{-1}$
300 ¹, which is higher than the experimental one. The difference between theoretical and experimental
301 values can be attributed to several factors as discussed for FcMeOH, but other issues can also
302 affect the process in the case of the metal deposition. Indeed, for Au the deposition of the metal
303 occurs through its reduction into Au(+I) (as described by eq. 4) followed by the formation of
304 Au(0) by dismutation. This phenomenon occurs after adsorption of gold complexes onto active
305 sites, leading to the formation of multiple entities assimilated to nanoparticles [22]. The
306 deposition of Au occurs in parallel to the formation of Au(+III), thus a fraction of the sample
307 doesn't turn into solid and it is removed from the system without any treatment and being

308 recovered. For Pd, the mechanism of growth of metallic deposit is discussed in the literature since
309 it does not seem to correspond to a simple model where the ion is reduced on existing nuclei sites
310 [25]. Depending on the applied potential, the growth of Pd can be described by different models
311 [26] and only for high overpotential reduction value, bulk Pd deposit is observed [27]. In our
312 case, the applied potential during the reduction step of chronoamperometric experiment
313 corresponds to high overpotential, which is in favor of the formation of bulk metals. Moreover,
314 since this potential value is high, reduction of the solvent overlaps the metal reduction and this
315 leads to loss of performances of the electrode, explaining the impossibility to reach high
316 depletion yield. The fact is that as soon as the deposition process begins for a given metal, the
317 formation of the metal on the C/PDMS electrodes can induce a change in the reduction of metal
318 complexes. This was evaluated by measuring the mean current of reduction of each metal on C-
319 PDMS electrode previously modified with the same metal deposit. As illustrated in Figure 10, the
320 mean current of metal ion reduction obtained by chronoamperometry on C-PDMS or on metal
321 modified C-PDMS electrode are represented as a function of the applied potential (with blank
322 subtraction).

323 **Figure 10 – Mean current value obtained by chronoamperometry as a function of the**
324 **potential for (a) 1000 $\mu\text{mol L}^{-1}$ Pd in 0.1 mol L^{-1} HCl and (b) 500 $\mu\text{mol L}^{-1}$ Au in 0.14 mol L^{-1}**
325 **HCl at WE_{DEP} C-PDMS electrode (open square) and WE_{DEP} C-PDMS modified electrode**
326 **(solid square). Metal deposits were performed at -1 V/C-PDMS on WE_{DEP} for 120s without**
327 **flow. The same experiments with WE_{det} let to similar results (data not shown).**

328 In the case of Au, the current related to the reduction of the metal complex is higher on Au-
329 modified electrode than on C-PDMS for all the considered potential range. This can be attributed
330 to a higher active surface or to a thermodynamically more favourable deposition on Au
331 substrates. Thus, thin layered gold modification of C-PDMS electrode material is recommended
332 to enhance the performances of the process. In the case of Pd, the current related to Pd reduction

333 is clearly lower on Pd-modified electrode than on C-PDMS electrode for all the considered
334 potential range. This can be explained by the fact that Pd acts as a catalyst at such a high
335 reduction potential for the hydroxonium reduction. The reduction of Pd is thus overlapping with
336 that of protons. This leads to a decrease of the deposition rate and potentially explains why the
337 depletion yield cannot be larger. All these results demonstrate also why the depletion yield for Au
338 is much higher than for Pd (Figure 8).

339

340 **4. Conclusion**

341 The depletion of precious metals on home-made reversible microchips was demonstrated with the
342 integration of graphite/PDMS microelectrodes within microfluidic channels. After
343 characterization of process performances with a model electroactive probe (FcMeOH), this
344 device was applied for the electrodeposition of Au and Pd, with a depletion yield of up to 89%
345 for Pd and 71% for Au. These values were obtained for low metal concentration ($25 \mu\text{mol L}^{-1}$),
346 which is in the range of those expected from leach liquors of PCBs wastes, undergoing a
347 hydrometallurgical treatment. In order to further increase the depletion yield, other experimental
348 parameters can be explored, such as the electrode size so as to increase the overall active surface
349 and to overcome surface defaults. Such a microchip thus opens the way for real leach liquor
350 treatment from the waste electric equipment recycling industry or for wastewater purification. To
351 do so, a focus is therefore recommended on the optimization of the confinement on which this
352 process is based, so as to increase the depletion yield. Indeed, this setup can be implemented on
353 industrial scale provided that the confinement is ensured and optimized. It can also be used as a

354 promising tool for the depletion of contaminant species whose removal rests on their
355 electrochemical reactivity, such as organic pollutants or inorganic ions.

356

357 **5. Acknowledgements**

358 This work was supported by the French Environment and Energy Management Agency
359 (ADEME) and the Chaire “Mines Urbaines” from ParisTech foundation, supported by Eco-
360 systèmes. This work has received support of “Institut Pierre-Gilles de Gennes” (Laboratoire
361 d’excellence: ANR-10-LABX-31, “Investissements d’avenir”: ANR-10-IDEX-0001-02 PSL and
362 Equipement d’excellence: ANR-10-EQPX-34).

363 **6. Reference**

- 364 [1] Rapport annuel du registre des Déchets d’Équipements Électriques et Électroni..., ADEME.
365 (n.d.). [http://www.ademe.fr/rapport-annuel-registre-dechets-dequipements-electriques-](http://www.ademe.fr/rapport-annuel-registre-dechets-dequipements-electriques-electroniques-deee-donnees-2015)
366 [electroniques-deee-donnees-2015](http://www.ademe.fr/rapport-annuel-registre-dechets-dequipements-electriques-electroniques-deee-donnees-2015) (accessed August 22, 2017).
- 367 [2] V. Goodship, A. Stevels, J. Huisman, Waste Electrical and Electronic Equipment (WEEE)
368 Handbook, Woodhead Publishing, 2019.
- 369 [3] B. Ghosh, M.K. Ghosh, P. Parhi, P.S. Mukherjee, B.K. Mishra, Waste Printed Circuit
370 Boards recycling: an extensive assessment of current status, *Journal of Cleaner Production*.
371 94 (2015) 5–19. <https://doi.org/10.1016/j.jclepro.2015.02.024>.
- 372 [4] P.O. of the E. Union, Report on critical raw materials and the circular economy., (2018).
373 [https://publications.europa.eu/en/publication-detail/-/publication/d1be1b43-e18f-11e8-b690-](https://publications.europa.eu/en/publication-detail/-/publication/d1be1b43-e18f-11e8-b690-01aa75ed71a1/language-en/format-PDF)
374 [01aa75ed71a1/language-en/format-PDF](https://publications.europa.eu/en/publication-detail/-/publication/d1be1b43-e18f-11e8-b690-01aa75ed71a1/language-en/format-PDF) (accessed December 20, 2018).
- 375 [5] M. Kaya, Recovery of metals and nonmetals from electronic waste by physical and
376 chemical recycling processes, *Waste Management*. 57 (2016) 64–90.
377 <https://doi.org/10.1016/j.wasman.2016.08.004>.
- 378 [6] G.M. Whitesides, The origins and the future of microfluidics, *Nature*. 442 (2006) 368–373.
379 <https://doi.org/10.1038/nature05058>.
- 380 [7] Les micro-réacteurs : opportunités et applications pour les industries chimiques - 2007,
381 Direction Générale des Entreprises (DGE). (n.d.). [https://www.entreprises.gouv.fr/secteurs-](https://www.entreprises.gouv.fr/secteurs-professionnels/micro-reacteurs-opportunités-et-applications-pour-industries-chimiques-2007)
382 [professionnels/micro-reacteurs-opportunités-et-applications-pour-industries-chimiques-2007](https://www.entreprises.gouv.fr/secteurs-professionnels/micro-reacteurs-opportunités-et-applications-pour-industries-chimiques-2007)
383 (accessed April 24, 2019).
- 384 [8] P.L. Suryawanshi, S.P. Gumfekar, B.A. Bhanvase, S.H. Sonawane, M.S. Pimplapure, A
385 review on microreactors: Reactor fabrication, design, and cutting-edge applications,

- 386 Chemical Engineering Science. 189 (2018) 431–448.
387 <https://doi.org/10.1016/j.ces.2018.03.026>.
- 388 [9] D. M. Roberge, M. Gottsponer, M. Eyholzer, N. Kockmann, Industrial design, scale-up, and
389 use of microreactors, *Chimica Oggi*. 27 (2009) 8–11.
- 390 [10] M. Yew, Y. Ren, K.S. Koh, C. Sun, C. Snape, A Review of State-of-the-Art Microfluidic
391 Technologies for Environmental Applications: Detection and Remediation, *Glob. Chall.* 3
392 (2019) 1800060. <https://doi.org/10.1002/gch2.201800060>.
- 393 [11] C. Tian, Q. Tu, W. Liu, J. Wang, Recent advances in microfluidic technologies for organ-
394 on-a-chip, *Trac-Trends Anal. Chem.* 117 (2019) 146–156.
395 <https://doi.org/10.1016/j.trac.2019.06.005>.
- 396 [12] T. Watanabe, S. Shibano, H. Maeda, A. Sugitani, M. Katayama, Y. Matsumoto, Y. Einaga,
397 Fabrication of a Microfluidic Device with Boron-doped Diamond Electrodes for
398 Electrochemical Analysis, *Electrochimica Acta*. 197 (2016) 159–166.
399 <https://doi.org/10.1016/j.electacta.2015.11.035>.
- 400 [13] R. Oliveira, C. Sella, C. Souprayen, E. Ait-Yahiatene, C. Slim, S. Griveau, L. Thouin, F.
401 Bedioui, Development of a flow microsensor for selective detection of nitric oxide in the
402 presence of hydrogen peroxide, *Electrochimica Acta*. 286 (2018) 365–373.
403 <https://doi.org/10.1016/j.electacta.2018.07.158>.
- 404 [14] C. Amatore, N. Da Mota, C. Sella, L. Thouin, Theory and Experiments of Transport at
405 Channel Microband Electrodes under Laminar Flows. 1. Steady-State Regimes at a Single
406 Electrode, *Anal. Chem.* 79 (2007) 8502–8510. <https://doi.org/10.1021/ac070971y>.
- 407 [15] C. Amatore, N. Da Mota, C. Lemmer, C. Pebay, C. Sella, L. Thouin, Theory and
408 Experiments of Transport at Channel Microband Electrodes under Laminar Flows. 2.
409 Electrochemical Regimes at Double Microband Assemblies under Steady State, *Anal.*
410 *Chem.* 80 (2008) 9483–9490. <https://doi.org/10.1021/ac801605v>.
- 411 [16] R. Oliveira, F. Bento, C. Sella, L. Thouin, C. Amatore, Direct Electroanalytical Method for
412 Alternative Assessment of Global Antioxidant Capacity Using Microchannel Electrodes,
413 *Anal. Chem.* 85 (2013) 9057–9063. <https://doi.org/10.1021/ac401566w>.
- 414 [17] K. Anwar, T. Han, S.M. Kim, Reversible sealing techniques for microdevice applications,
415 *Sensors and Actuators B: Chemical*. 153 (2011) 301–311.
416 <https://doi.org/10.1016/j.snb.2010.11.002>.
- 417 [18] R.S. Martin, A.J. Gawron, S.M. Lunte, C.S. Henry, Dual-Electrode Electrochemical
418 Detection for Poly(dimethylsiloxane)-Fabricated Capillary Electrophoresis Microchips,
419 *Anal. Chem.* 72 (2000) 3196–3202. <https://doi.org/10.1021/ac000160t>.
- 420 [19] J.M. Petroni, B.G. Lucca, V.S. Ferreira, Simple approach for the fabrication of screen-
421 printed carbon-based electrode for amperometric detection on microchip electrophoresis,
422 *Analytica Chimica Acta*. 954 (2017) 88–96. <https://doi.org/10.1016/j.aca.2016.12.027>.
- 423 [20] J. Gouyon, F. d'Orlyé, S. Griveau, F. Bedioui, A. Varenne, Characterization of home-made
424 graphite/PDMS microband electrodes for amperometric detection in an original reusable
425 glass-NOA®-PDMS electrophoretic microdevice, *Electrochimica Acta*. 329 (2020) 135164.
426 <https://doi.org/10.1016/j.electacta.2019.135164>.
- 427 [21] C. Cannes, F. Kanoufi, A. J Bard, Cyclic voltammetry and scanning electrochemical
428 microscopy of ferrocenemethanol at monolayer and bilayer-modified gold electrodes,
429 *Journal of Electroanalytical Chemistry*. 547 (2003) 83–91. [https://doi.org/10.1016/S0022-0728\(03\)00192-X](https://doi.org/10.1016/S0022-0728(03)00192-X).
- 430

- 431 [22] L. Komsijska, G. Staikov, Electrocrystallization of Au nanoparticles on glassy carbon from
432 HClO₄ solution containing [AuCl₄]⁻, *Electrochimica Acta*. 54 (2008) 168–172.
433 <https://doi.org/10.1016/j.electacta.2008.08.013>.
- 434 [23] G. Chang, Y. Luo, W. Lu, X. Qin, A.M. Asiri, A.O. Al-Youbi, X. Sun, Electrodeposition
435 Fabrication of Pd Nanoparticles on Glassy Carbon Electrode Towards Methanol Oxidation
436 Application, *Current Research in Nanotechnology*. 4 (2013) 1–7.
437 <https://doi.org/10.3844/ajns.2013.1.7>.
- 438 [24] E. Kim, M. Kim, J. Lee, B.D. Pandey, Selective recovery of gold from waste mobile phone
439 PCBs by hydrometallurgical process, *Journal of Hazardous Materials*. 198 (2011) 206–215.
440 <https://doi.org/10.1016/j.jhazmat.2011.10.034>.
- 441 [25] S. Gu, X. Wang, Y. Wei, B. Fang, Mechanism for nucleation and growth of electrochemical
442 deposition of palladium(II) on a platinum electrode in hydrochloric acid solution, *Sci. China*
443 *Chem.* 57 (2014) 755–762. <https://doi.org/10.1007/s11426-013-5026-2>.
- 444 [26] A. Alvarez, D.R. Salinas, Formation of Cu/Pd bimetallic crystals by electrochemical
445 deposition, *Electrochimica Acta - ELECTROCHIM ACTA*. 55 (2010) 3714–3720.
446 <https://doi.org/10.1016/j.electacta.2010.01.076>.
- 447 [27] A. Sahin, Q. Huang, J.M. Cotte, B.C. Baker-O’Neal, Electrochemical Palladium Deposition
448 for Reducing Critical Dimensions in Nanostructures, *J. Electrochem. Soc.* 161 (2014)
449 D697–D703. <https://doi.org/10.1149/2.0851412jes>.
- 450